Radar Signatures and Ocean Color Response of Internal Wave-Wave Interactions Between the Lombok Strait and the Flores Sea

I Wayan Gede Astawa Karang [1,2*], I Gede Hendrawan[1,2], I Made Dwita Krisnanda[1], I Gusti Bagus Sila Dharma[1], I Wayan Krisna Eka Putra[3], I Made Mahendra Wicaksana Karang[1], and Jonson Lumban Gaol[4]

[1]Faculty of Marine Science and Fisheries, Udayana University, Bali, Indonesia

[2]Centre for Remote Sensing and Ocean Sciences (CReSOS), Udayana University, Bali, Indonesia

[3]Universitas Pendidikan Ganesha, Bali, Indonesia

[4]Department of Marine Science and Technology, Bogor Agricultural University, Indonesia

*gedekarang@unud.ac.id

Abstract *Many internal solitary wave (IWs) patterns have been observed in satellite images, particularly in the Lombok Strait and Flores Sea. However, there are no studies that have been made on internal wave interaction patterns in this area. Interactions between internal waves may generate unusually large amplitudes within their convergence zones, which can pose significant risks to underwater structures. This study examines the surface expressions of internal wave–wave interactions detected in satellite images of the Flores Sea. The data used are a Sentinel-1 SAR image (October 28, 2018) and a GCOM-C optical image (October 29, 2018). The methods applied to both images consist of preprocessing, image enhancement, and pattern extraction. The analysis of both images indicated the presence of internal wave packets propagating in the Lombok Strait and Flores Sea with soliton wavelengths of 3.9-5.0 km and phase velocities of 2.5-26 m/s. Analysis of the wave interactions revealed a clear grid-like interaction pattern, formed by the meeting of two non-linear internal wave packets originating from different sources. The first packet, propagating northward, was identified as originating from the Lombok Strait, while the second packet was propagating from the northeast. This ^woven^ pattern is a manifestation of a series of X-type interactions, forming rhomboid-shaped cells on the sea surface, with each grid cell area ranging from 19.3 - 21.4 km2. From visual analysis of the imagery, the angle between the wave crests is estimated to be approximately 115^0 , indicating an interaction angle between the wave propagation directions of approximately 65^0. This study indicates that both radar and optical are capable of detecting the surface manifestation of complex interactions by two or more internal wave packets. Further studies will focus on quantitative analysis of wave parameters to understand the impact of these interactions on local marine productivity.*

Keywords: Internal Wave-Wave Interaction, SAR, grid-like interaction pattern, Flores Sea, Lombok Strait

1. Introduction

Internal waves are waves that occur within the ocean's interior. Internal wave can be generated by disturbances of pycnocline or interface layers. Under typical oceanic conditions, the vertical gradients of temperature and salinity in the upper layer are quite pronounced. When any form of disturbance affects the pycnocline, it generally triggers oscillations that travel away from

their source region as internal waves. Such disturbances can arise from several mechanisms, ranked roughly by their significance: (1) tidal movements of stratified water interacting with bathymetric features such as islands, seamounts, or continental shelf slopes; (2) atmospheric influences, including variations in barometric pressure and surface wind stress; (3) interactions between surface and internal waves; and (4) other processes capable of displacing the pycnocline (Apel, 1988). Each disturbance may produce either an individual internal wave or a complete packet of waves.

In the ocean, internal wave packets frequently interact with one another during propagation. A common and intriguing phenomenon seen often in satellite photos, both synthetic aperture radar (SAR) and optical images taken in partially cloud-free conditions, is the consequent internal wave-wave interaction pattern. Internal wave trains often merge to form a larger packet when their propagation directions are nearly aligned. Certain interaction patterns exhibit noticeable phase changes when their propagation directions are not particularly close to one another, whilst other patterns do not exhibit any phase shifts and suggest that interactions only slightly affect internal wave packets. Studying interaction patterns is challenging because to their complicated dynamics and limited geophysical observations (Xue et al., 2014).

The Indonesian archipelagic waters play a crucial role in the global climate system, functioning as the only low-latitude oceanic gateway that connects the Indian and Pacific Oceans a system known as the Indonesian Throughflow (Arlindo) (Gordon, 2005). The Arlindo not only modulates the heat and water mass balances of both oceans, but also significantly influences regional and global climate variability, including phenomena such as the El Niño-Southern Oscillation (ENSO) (Sprintall et al., 2014). Within this complex system, key straits such as the Lombok Strait serve as crucial gateways that regulate the flow of water masses, while also serving as locations where small- to meso-scale oceanographic processes produce large-scale impacts.

The generation of intense nonlinear internal waves represents one of the most energetic oceanic phenomena occurring in the Lombok Strait. These waves are formed when strong barotropic tidal currents interact with steep seafloor topography, particularly the sill in the southern part of the strait (Raharja et al., 2021; Karang et al., 2010). Once formed, these internal wave packets propagate away from their source, primarily northward toward the Flores Sea, carrying significant amounts of energy and momentum (Susanto et al., 2005). The propagation and dissipation of this wave energy is a key mechanism for vertical mixing within the water column,

a process essential for the distribution of heat, salinity, and nutrients, and supports aquatic biological productivity (Alford et al., 2015).

As they propagate, internal waves from the Lombok Strait can encounter and interact with other waves generated from local sources in the Flores Sea, creating a highly complex wave field. These wave-wave interactions can produce complex interference patterns, nonlinear energy transfer, and significantly increased energy dissipation (Apel, 1987). Understanding the dynamics of these interactions is crucial, but direct field observations over large areas are often difficult and expensive.

Satellite remote sensing technology offers an effective solution for observing the surface manifestations of these subsurface phenomena at the synoptic scale. Synthetic Aperture Radar (SAR) imagery is highly effective in mapping the physical structure of internal waves by detecting changes in sea surface roughness (Alpers, 1985), while ocean color sensors can provide clues to the biogeochemical responses of the waters, such as increases in chlorophyll-a concentrations due to nutrient uptake (da Silva, 2002).

So many authors used optical sensor and SAR to study the internal waves characteristics in the Flores Sea and Lombok Strait (Susanto et al., 2005; Karang et al, 2012; 2019) but none of this study about the interactions between the waves. This study provided the results of image analyses of the characteristic of wave-wave interactions of internal waves between Lombok Strait and Flores Sea using SAR Sentinel-1 and GCOM-C optical data.

2. Literature Review

Remote sensing observations of internal waves

One of the major challenges in internal wave observation lies in the difficulty of achieving clear results through in-situ measurements. Numerous environmental factors including bathymetry, temporal variations, seasonal changes, wind, and temperature can alter the morphology of the waves, occasionally causing them to dissipate or leave little observable evidence (Chen-Yuan Chen, 2012). Prior to the advent of satellite remote sensing, internal wave occurrences in the ocean were largely underestimated because synoptic-scale observations were unavailable. Data acquired from satellite instruments such as scatterometers, altimeters, infrared radiometers, and ocean color sensors have provided new opportunities to observe and quantify ocean dynamics explaining the movement of water masses and to examine the mechanisms of air sea energy exchange. The satellite-derived measurements revealed several unexpected findings for physical oceanographers, such as

the detection of internal tides in the open ocean, the identification of a highly dynamic surface ocean dominated by eddies, and the observation of global sea-level trends with millimeter per year precision. The integration of satellite data, in situ measurements, and numerical models has transformed physical oceanography into a truly global science with enhanced predictive skill.

Internal waves represent one of the most readily identifiable oceanographic features in remote sensing imagery. Their distinct patterns alternating light and dark quasi-linear bands have been observed in sea-surface photographs, multispectral radiometer imagery, and both real and SAR data. Synthetic Aperture Radar (SAR) became the most important remote sensors for internal wave detection. Beginning with the launch of Seasat in 1978 and continuing through the European Remote Sensing (ERS-1 and ERS-2) and Canadian RADARSAT missions, SAR imagery has been extensively utilized to detect and map internal wave patterns over continental shelves and in the open ocean. Therefore, SAR data have been increasingly utilized in the study of internal waves, especially since the advent of advanced SAR platforms such as JAXA's ALOS PALSAR and Copernicus's Sentinel-1 (Matthews et al., 2011; Karang et al., 2012; Mitnik, 2008; Chonnaniyah et al., 2021).

In satellite imagery, internal waves manifest as alternating bright and dark bands on the ocean surface. These features result from vertical displacements of the pycnocline or thermocline and from surface current variations, where zones of convergence and divergence form in response to the underlying internal wave motion (Jackson, 2004; Klemas, 2012). Key parameters of internal waves, such as their characteristic half width, crest length, number and spacing of waves, propagation direction, and phase speed, can be extracted from single or sequential satellite imagery (Zheng et al., 2001b, Klemas, 2012). By incorporating internal wave parameters into oceanographic models, researchers have successfully derived essential physical characteristics, such as the depth of the ocean's mixed layer (Brandt et al., 1996; Jones, 1995; Kara et al., 2003; Li et al., 2000; Porter and Thompson, 1999).

Internal waves and their surface manifestations have also been observed by multispectral and visible band. Modulations of sunglint radiance at the ocean surface induced by internal waves have been observed in numerous satellite images acquired from missions such as Gemini, Apollo, DMSP (Defense Meteorological Satellite Program), Landsat, SPOT,

NOAA, and the Space Shuttle (Soules, 1970; Apel et al., 1975; Pingree and New, 1995, and Hennings and Metzner, 1996). Jackson used Moderate Resolution Imaging Spectroradiometer (MODIS) photos for global internal wave identification (Jackson, 2007), and Zhao et al. used SPOT-3 satellite optical images to examine the polarity change of ISWs along the continental shelf of the northern South China Sea (Zhao et al., 2003). In their study, Huang and Zhao identified and quantified the characteristic features of a typical internal solitary wave (ISW) occurring in the deep waters of the northern South China Sea. Karang et al (2019) used Himawari-8 dataset to observe internal solitary waved in the Flores Sea.

3. Methodology

Research location

The study focuses on the Flores Sea, north of the Lombok Strait and the Nusa Tenggara islands (Figure 1). This oceanographically significant region is a primary pathway for the ITF and is characterized by complex bathymetry, including numerous sills and basins that serve as generation sites for internal waves.

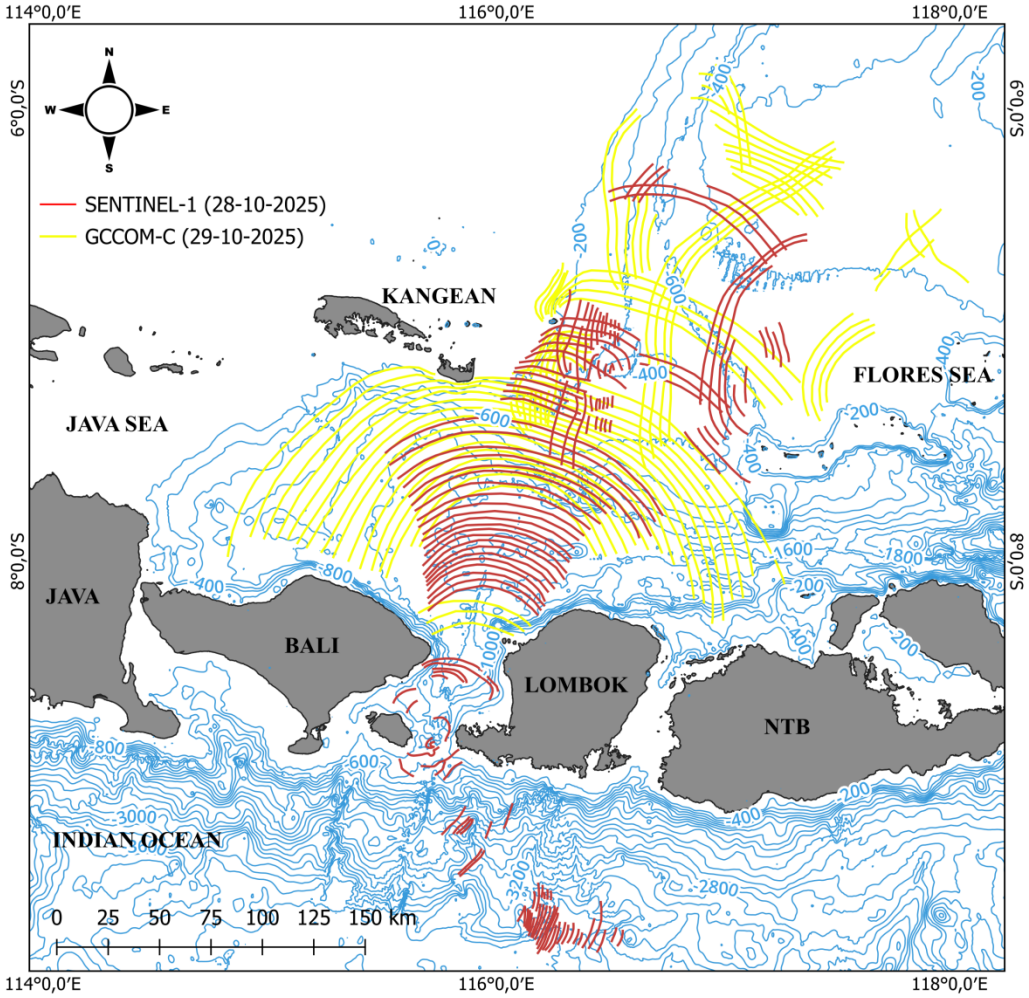

Figure 1: A map of the study area. The numbers on the isobaths are in meters. The bathymetric contours derived from General Bathymetric Chart of the Oceans (GEBCO) data set, https://www.gebco.net/. The red lines are internal waves pattern revealed on the Sentinel-1 SAR image, and the yellow line are Internal solitary waves pattern revealed on the GCOM-C image.

Dataset

This study used imagery from the Sentinel-1B satellite acquired on October 28, 2018, and imagery from the GCOM-C (Global Change Observation Mission – Climate) satellite acquired on October 29, 2018. Sentinel-1 is part of the Copernicus program developed by the European Space Agency (ESA).

The Sentinel-1 constellation includes two polar-orbiting satellites, Sentinel-1A and Sentinel-1B, which provide all weather, day and night Synthetic Aperture Radar (SAR) observations operating at C-band frequencies. Both satellites offer four image acquisition

modes with varying resolutions (down to approximately 5 meters) and coverage ranges (up to 400 km) (Torres et al., 2012). Sentinel-1A, the first satellite of the Copernicus Sentinel-1 mission, was launched in April 2014, followed by Sentinel-1B in 2016. Both satellites have a 12-day equatorial return cycle, with an orbital phase difference of 180°, allowing for more frequent and broader observation coverage. The primary instrument carried is a C-band SAR with a center frequency of 5.405 GHz, capable of recording data in dual polarization modes (HH + HV or VV + VH). This system operates through one transmission chain and two parallel reception chains for horizontal (H) and vertical (V) polarization. In operation, Sentinel-1 provides four main acquisition modes: Stripmap, Interferometric Wide Swath (IW), Extra-Wide Swath (EW), and Wave Mode (WV). From these modes, the resulting products include Level-1 Single Look Complex (SLC), Level-1 Ground Range Detected (GRD), and Level-2 Ocean products, which are widely used in ocean dynamics monitoring and satellite oceanography (Tao et al., 2022). In this study, Level-1B Ground Range Detected (GRD) products from Sentinel-1A Interferometric Wide (IW) mode with VV polarization (decibel gamma0) were used for the identification of internal waves. Sentinel-1 data were obtained from the Copernicus Open Access Hub (https://browser.dataspace.copernicus.eu/), with a spatial resolution of approximately 450 m.

Launched on December 23, 2017, the GCOM-C (SHIKISAI) satellite operates in a sun-synchronous polar orbit at an altitude of 800 km, with an inclination of 98.6° and a descending node at approximately 10:30 a.m. local time. Its primary sensor, the Second-generation Global Imager (SGLI), has been conducting continuous observations since January 1, 2018. The instrument features 17 spectral bands covering wavelengths from the near-ultraviolet (380 nm) to thermal infrared (12 μm), including two polarization channels centered in the red and near-infrared domains. The spatial resolution of SGLI varies: channels VN01–VN11, SW03, and TI01–02 have a 250 m instantaneous field of view (IFOV) for global land and coastal areas, while for open sea areas, the resolution is reduced to 1 km using the onboard averaging function (Shimoda, 2011; Tanaka et al., 2010).

In this study, Level 1B products of GCOM-C SGLI were used for the identification of internal waves in the study area. The GCOM-C satellite data were obtained from the Globe Portal System (http://gportal.jaxa.jp/gpr/). Specifically, Band 6 (green), with a wavelength of 565 nm and a spatial resolution of 250 m, was utilized. The imagery was acquired by the Second-generation Global Imager (SGLI) sensor.

Data Preprocessing

The next step involved visual adjustments to enhance image quality and readability for the identification of internal waves. Two types of satellite data were used in this study: Level-1B GRD raw products from Sentinel-1B IW VV - decibel gamma0, and GCOM-C SGLI Level 1B data, both selected in their pre-processed form to minimize additional processing. Sentinel-1B imagery ensured standard radiometric calibration and geometric corrections had been applied, while GCOM-C SGLI Level 1B data had already received radiometric and geometric corrections at the provider level.

The study focused on visual identification and digitization of internal wave patterns rather than quantitative ocean analysis, complex preprocessing (e.g., atmospheric correction for SGLI or advanced SAR noise correction) was unnecessary. Contrast enhancement was performed in QGIS through the Symbology menu. Images were displayed as Singleband grayscale, with the Contrast Enhancement method set to Stretch to Min-Max. The crucial step was manually adjusting the Min/Max Value Settings to map pixel values optimally to the color scale, improving the visibility of internal wave features for accurate digitization of crest lines.

Image Processing

Internal Wave Extraction

Internal Wave Feature Extraction Internal wave packets were manually digitized in QGIS using a New Shapefile Layer to create polylines. Manual digitization using the Advanced Digitizing Toolbar was chosen due to the varied and irregular visual patterns of the waves, which are difficult for automated algorithms to identify. Each visible wave crest was traced to create a vector representation of the wave field.

Propagation Direction

The propagation direction (θ_{prop}) of internal waves was quantified using the Azimuth and Distance Calculator plugin in QGIS. Azimuth refers to the angle measured in a clockwise direction from a reference meridian to a specific point on the horizon (Barazzetti, 2025). The crest lines of internal waves were first delineated through manual digitization of satellite imagery. Subsequently, a vector was drawn perpendicular to each crest line, oriented toward the direction of wave propagation. The Azimuth and Distance Calculator plugin was then employed to compute the Real Azimuth of these vectors, representing the true directional bearing relative to geographic north. In this convention, 0° corresponds to north, 90° to east,

180° to south, and 270° to west. To obtain the acute propagation angle (θ_{prop}), the *Real Azimuth* was transformed according to the following equation.

$$\theta prop = \begin{cases} \textbf{Real azimuth}, & \textbf{if Real Azimuth} \leq \textbf{180°} \\ \textbf{Real azimuth} - \textbf{360°}, & \textbf{if Real Azimuth} \geq \textbf{180°} \end{cases}$$

Interaction Angle Calculation

To quantify the interaction geometry, two angles were calculated: Crest Angle (θ_{crest}): This is the angle formed by the direct physical intersection of the two crest lines from different wave packets. This angle was measured using the Measure Angle tool in QGIS. Wave-wave interaction angle (ψ): this is the true physical angle between the propagation directions of the two wave packets. As propagation direction is perpendicular to the crest line, this angle was calculated using the standard geometric relationship: $\psi = 180^{o} - \theta_{crest}$.

4. Results and Discussion

Multi sensor Observation of Internal Wave's Packet

The analysis of SAR and GCOM-C images confirmed the presence of extensive and complex internal wave fields in the Flores Sea. Both the Sentinel-1 SAR image (Figure 2a) and the GCOM-C optical image (Figure 3a) successfully captured the surface manifestations of these waves, demonstrating the capability of both radar and optical sensors to detect such phenomena. The digitized wave crests (Figure 1) reveal two primary wave systems. The most prominent, Packet 1 (Figures 2b and 3b), consists of a large, coherent packet of non-linear waves propagating northward with θ_{prop} values of 12° and 3°, respectively. Its curved crests and apparent origin are consistent with generation from the main sill in the Lombok Strait, a well-known generation site. Analysis indicates that this packet has soliton wavelengths ranging from 3.9 to 5.0 km.

A second group of wave packets (Packets 2, 4, and 5) is observed propagating from the northeast, likely originating from local bathymetric features within the Flores Sea. These packets are less uniform than Packet 1 and appear to be on a direct collision course with it (Figures 2c and 3c). The azimuth and propagation angles (θ_{prop}) derived from Sentinel-1 imagery (Table 1), indicate distinct propagation directions among the wave packets. Packets 1, 3, and 5 propagate toward the northeast (θ_{prop} = 12°, 13°, and 21°), whereas Packets 2 and 4 have propagation angles of –84° and –59°, indicating northwestward propagation. These opposing directions suggest the presence of a wave–wave interaction zone, as illustrated in

Figure 2c. Similar internal wave patterns were also identified in the GCOM-C imagery (Figure 3). The image clearly shows several packets distributed across the Flores Sea with distinct propagation directions. Packets 1, 3, and 6 propagate toward the northeast (θ_{prop} = 3°, 11°, and 73°), while Packets 2, 4, and 5 propagate toward the northwest (θ_{prop} = –72°, –60°, and –84°). The overlapping regions between northeastward and northwestward packets, as shown in Figure 3c, mark possible zones of wave–wave interaction, consistent with those identified in the Sentinel-1 imagery.

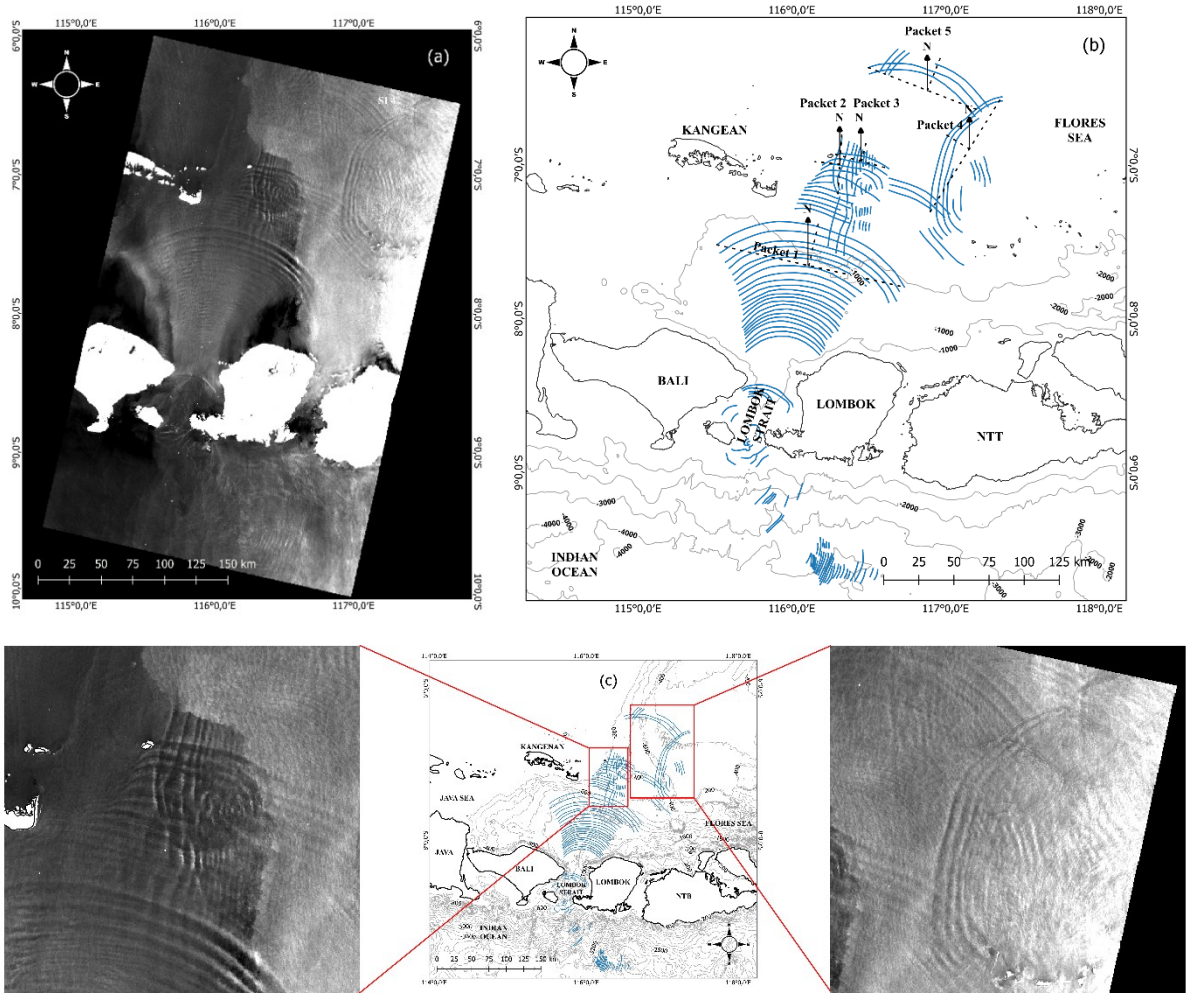

Figure 2: a. Internal wave packet appeared on Sentinel-1 SAR image, b. direction identification, c. wave-wave interaction

Table 1: Propagation Angles of Sentinel-1 Packets

Packet	Real Azimuth	θ_{prop}
1	12°	12°
2	275°	-85°
3	13°	13°
4	301°	-59°
5	21°	21°

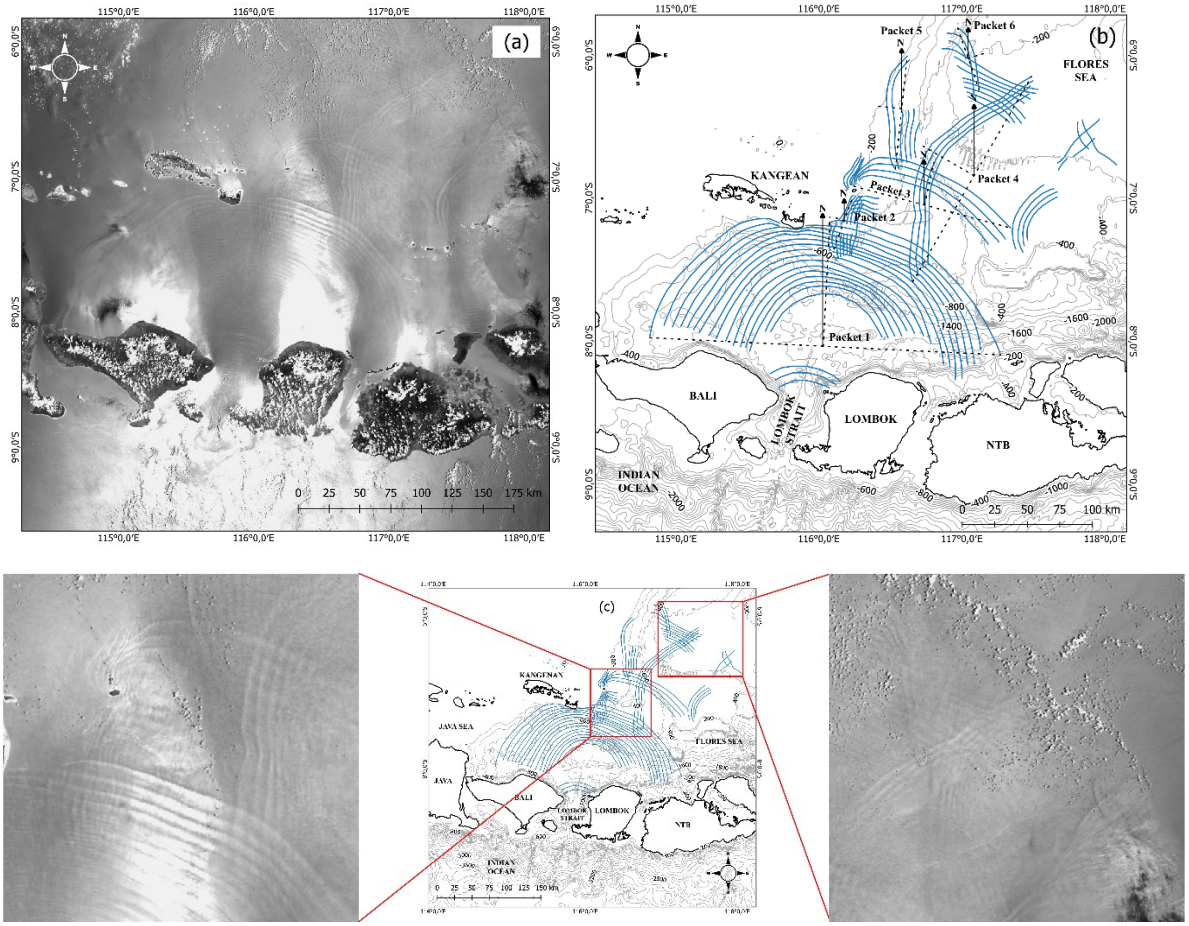

Figure 3: a. Internal wave packet appeared on GCOM-C image, b. direction identification, c. wave-wave interaction

Table 2: Propagation Angles of GCOM-C Packets

Packet	Real Azimuth	θ_{prop}
1	3°	3°
2	288°	-72°
3	11°	11°
4	300°	-60°
5	276°	-84°
6	73°	73°

Analysis of the Grid-Like Interaction Pattern

The most significant finding is the clear grid-like interaction pattern observed in the central part of the study area, where Packet 1 and the northeastern packets meet (Figures 2 and 3). Specifically, several interaction zones (SI1–SI5) were identified from Sentinel-1 image across the region (Figure 4a). SI1 represents the interaction between Packet 1 and Packet 2, forming the most prominent and well-defined grid structure. SI2 corresponds to the crossing

of Packet 3 and Packet 4, where the wave crests intersect at nearly perpendicular angles, producing a smaller but distinct X-type pattern. SI3 occurs between Packet 2 and Packet 3, showing partial interference features and less coherent intersections compared to SI1 and SI2. SI4 indicates the intersection between Packet 4 and Packet 5, where the overlapping crests are more diffuse, likely due to dissipation effects or differences in wave amplitude. SI5 appears at the northernmost part of the image and shows interaction between Packet 5 and an unclassified, weaker wavefront, possibly generated by secondary internal waves or reflected signals.

A total of eight internal wave interaction zones (SI1–SI8) were identified from the GCOM-C image (Figure 4b). SI1 corresponds to the interaction between Packet 1 and Packet 2, representing one of the strongest and clearest crossing patterns, consistent with the main interaction zone detected in the Sentinel-1 image. SI2 represents the intersection between Packet 1 and Packet 4. SI3 and SI4 correspond to interactions between Packet 2 and Packet 3, and between Packet 3 and Packet 4, respectively. SI5 marks the intersection between Packet 3 and Packet 5. SI6 and SI7 are associated with interactions involving one unidentified packet, possibly weak or decaying internal waves that were not clearly distinguishable in the imagery. SI8 appears to involve two unidentified wave fronts, producing a faint but visible interference pattern, likely representing the residual or secondary interactions between dispersed solitons.

This “woven” pattern is the surface manifestation of a complex interaction between multiple non-linear internal wave systems. It is not a new wave type, but rather the result of a series of X-type interactions. An X-type interaction occurs when two solitary waves cross each other, largely retaining their original form but undergoing a phase shift. The observed grid is formed as each crest from Packet 1 crosses each crest from the opposing packets, creating distinct, diamond-shaped “cells” on the sea surface with areas ranging from 19.3 to 21.4 km^2. Visual analysis of the crest angles within this grid (Figure 4) allows for geometric quantification, where the measured angle between intersecting crests ($\theta crest$) is approximately 115°. Using the formula $\psi = 180° - \theta crest$, the true physical interaction angle (ψ) between the two propagation directions is calculated to be approximately 65°.

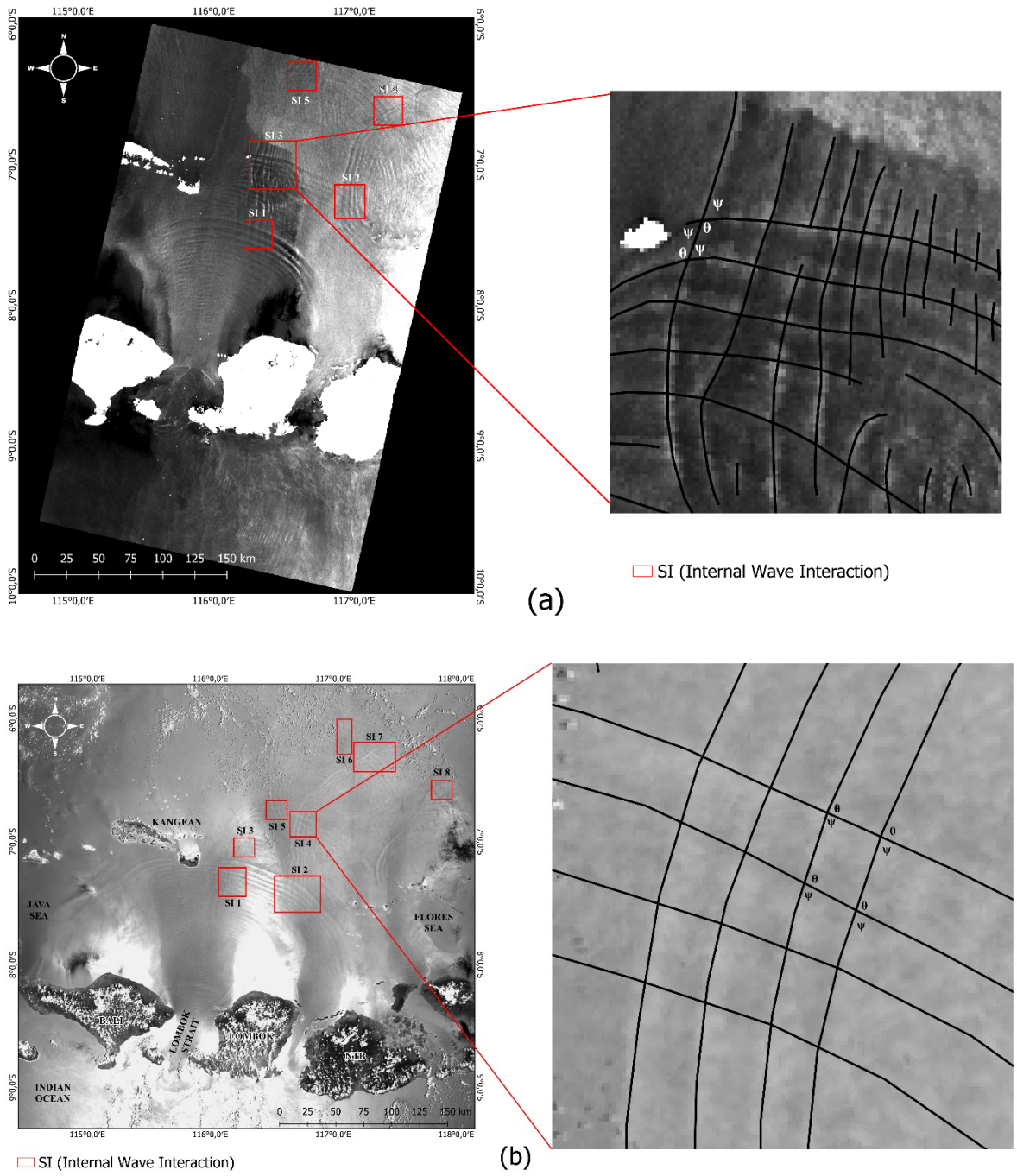

Figure 4: Interaction angle measurement on SAR image (a) and GCOM-C image (b)

5. Conclusion and Recommendation

This study successfully observed a large scale internal solitary waves packet, grid-like internal wave interaction in the Flores Sea using SAR and optical sensor approach. For the first time in this region, we provide clear evidence of the interaction between northward-propagating internal solitary waves from the Lombok Strait and packets originating from the Flores Sea. Both Sentinel SAR-1 and GCOM-C sensors are highly effective at capturing the complex surface signatures of these wave-wave interactions. Some interaction

characteristics can be directly observed, such as interaction zone, number of packets, pre-interaction and post-interaction angles. The observed "woven" pattern is a manifestation of a series of X-type interactions, forming rhomboid-shaped cells with an area of 19.3 - 21.4 km². The geometry of the interaction was quantified, with an angle between crests (θ_{crest}), resulting in a physical interaction angle (ψ). These findings highlight the Flores Sea as a critical "hotspot" for internal wave energy dissipation and mixing, driven by the collision of multiple energetic wave packets. This study lays the groundwork for future research, which will focus on a quantitative analysis of wave parameters and the corresponding ocean color response to understand the direct impact of these interactions on local marine productivity.

Acknowledgement

We would like to thank the Copernicus Data Space Ecosystem (https://browser.dataspace.copernicus.eu/) for access Sentinel-1 imagery and GEBCO (http://www.gebco.net) for access bathymetry data. This research was supported by the Hibah Penelitian Unggulan Udayana (PUU) grant from the LPPM, Udayana University for the year 2025.

References

Alford, M. H., Peacock, T., MacKinnon, J. A., Nash, J. D., Buijsman, M. C., Centurioni, L. R., ... & Tang, T. Y. (2015). The formation and fate of internal waves in the South China Sea. *Nature*, *521*(7550), 65–69. https://doi.org/10.1038/nature14399

Alpers, W. (1985). Theory of radar imaging of internal waves. *Nature*, *314*(6008), 245–247.

Apel, J. R. (1987). *Principles of ocean physics*. Academic Press.

Apel, J. R. (1988). Internal wave dynamics. In *Principles of ocean physics* (pp. 219-231). Academic Press.

Apel, J. R., Byrne, H. R., Proni, J. R., & Charnell, U. R. (1975). Observations of oceanic internal and surface wave from the Earth Resources Technology Satellite. *Journal of Geophysical Research*, *80*(6), 865–881.

Barazzetti, L. (2025). Revitalizing Astronomical Azimuth Determination: Integrating Modern Computing with Traditional Techniques. *Sensors*, *25*(6), 1871.

Chen, C. Y. (2012). A critical review of internal wave dynamics. Part 1 - Remote sensing and in-situ observations. Journal of Vibration and Control, 18(3), 417–436. https://doi.org/10.1177/1077546310395971

Chonnaniyah, Karang, I. W. G. A., & Osawa, T. (2021). Internal solitary waves propagation speed estimation in the northern-part of Lombok Strait observed by Sentinel-1 SAR and Himawari-8 images. IOP Conference Series: Earth and Environmental Science, 944, 012042.

da Silva, J. C. B. (2002). On the observability of internal tidal waves in remotely-sensed ocean colour data. Geophysical Research Letters, 29(12), 1569. https://doi.org/10.1029/2001GL013888

Gordon, A. L. (2005). Oceanography of the Indonesian seas and their throughflow. *Oceanography*, *18*(4), 14–27. https://doi.org/10.5670/oceanog.2005.01

Hennings, I., & Metzner, M. (1996). Sunglitter radiance modulation by internal waves. *German Journal of Hydrography*, *48*(2), 121–132.

Huang, X. D., & Zhao, W. (2014). Information of internal solitary wave extracted from MODIS image: A case in the deep water of northern South China Sea. *Periodical of Ocean University of China*, *44*, 19–23.

Jackson, C. (2007). Internal wave detection using the Moderate Resolution Imaging Spectroradiometer (MODIS). *Journal of Geophysical Research: Earth Surface*, *112*, C11012.

Jackson, C. R., & Apel, J. R. (Eds.). (2004). *Synthetic aperture radar (SAR) marine user's manual*. NOAA NESDIS Office of Research and Applications.

Karang, I. W. G. A., Chonnaniyah, & Osawa, T. (2019). Internal solitary wave observations in the Flores Sea using the Himawari-8 geostationary satellite. International Journal of Remote Sensing, 41(10), 3823–3840. https://doi.org/10.1080/01431161.2019.1693079

Karang, I. W. G. A., Nishio, F., Mitnik, L., & Osawa, T. (2012). Spatial-temporal distribution and characteristics of internal waves in the Lombok Strait area studied by Alos-Palsar images. Earth Science Research, 1(2), 11–22. https://doi.org/10.5539/esr.v1n2p11

Karang, I. W. G. A., Nishio, F., & Osawa, T. (2010). Estimation of tidal energy dissipation and vertical diffusivity in the Indonesian seas. International Journal of Remote Sensing and Earth Sciences, 7, 53–72.

Klemas, V. (2012). Remote sensing of ocean internal waves: An overview. Journal of Coastal Research, 28(3), 540–546.

Matthews, J. P., Aiki, H., Masuda, S., Awaji, T., & Ishikawa, Y. (2011). Monsoon regulation of Lombok Strait internal waves. Journal of Geophysical Research, 116, C05007.

Mitnik, L. M. (2008). Advanced Land Observing Satellite PALSAR observations of the oceanic dynamic phenomena in the coastal zone. Proceedings of the IEEE International Geoscience and Remote Sensing Symposium (IGARSS 2008). Boston, MA, USA.

Pingree, R. D., & New, A. L. (1995). Structure, seasonal development and sunglint spatial coherence of the internal tide on the Celtic and Armorican shelves and in the Bay of Biscay. *Deep-Sea Research Part I: Oceanographic Research Papers*, *42*(2), 245–284.

Raharja, I. M., Radjawane, I. M., & Hendrawan, I. G. (2021). Characteristic of tidal currents in the Lombok Strait using 3D FVCOM numerical model. *IOP Conference Series: Earth and Environmental Science*, *925*, 012002. https://doi.org/10.1088/1755-1315/925/1/012002

Shimoda, H. (2011, July). Overview of GCOM. In *2011 IEEE International Geoscience and Remote Sensing Symposium* (pp. 4134–4137). IEEE.

Soules, S. D. (1970). Sun glitter viewed from space. *Deep-Sea Research*, *17*(1), 191–195.

Sprintall, J., Gordon, A. L., Koch-Larrouy, A., Lee, T., Potemra, J. T., Pujiana, K., & Wijffels, S. E. (2014). The Indonesian seas and their role in the coupled ocean-climate system. *Nature Geoscience*, *7*, 487–492.

Susanto, R. D., Mitnik, L., & Zheng, Q. (2005). Ocean internal waves observed in the Lombok Strait. *Oceanography*, *18*(4), 80–87.

Tanaka, K., Okamura, Y., Amano, T., Hiramatsu, M., & Shiratama, K. (2010). Operation concept of the second-generation global imager (SGLI). In *Proceedings of SPIE, 7862, Earth Observing Missions and Sensors: Development, Implementation, and Characterization* (786209).

Tao, M., Xu, C., Guo, L., Wang, X., & Xu, Y. (2022). An internal waves data set from Sentinel-1 synthetic aperture radar imagery and preliminary detection. *Earth and Space Science*, *9*(12), e2022EA002528.

Torres, R., Snoeij, P., Geudtner, D., Bibby, D., Davidson, M., Attema, E., et al. (2012). GMES Sentinel-1 mission. *Remote Sensing of Environment*, *120*, 9–24.

Xue, J., Graber, H. C., Romeiser, R., & Lund, B. (2014). Understanding internal wave–wave interaction patterns observed in satellite images of the Mid-Atlantic Bight. *IEEE Transactions on Geoscience and Remote Sensing*, *52*(6), 3211–3219. https://doi.org/10.1109/TGRS.2013.2271777

Zhao, Z. X., Klemas, V. V., Zheng, Q. N., & Yan, X. H. (2003). Satellite observation of internal solitary waves converting polarity. *Geophysical Research Letters*, *30*(19), 1988.

Zheng, Q., Yuan, Y., Klemas, V., & Yan, X. H. (2001b). Theoretical expression for an ocean internal soliton synthetic aperture radar image and determination of the soliton characteristic half width. *Journal of Geophysical Research*, *106*(C12), 31415–31423.